JIANNAN HU
Department of Geography, Boston University, Boston, MA 02215, USA
Tel: 617-353-8845
Fax: 617-353-8399
Email: jiannan@crsa.bu.edu

JAN BOGAERT
Université Libre de Bruxelles, École Interfacultaire de Bioingénieurs, Laboratoire d'Écologie du Paysage, Avenue F.D. Roosevelt 50, Bruxelles, Belgique
Tel. 32-2-650-4897
Fax 32-2-650-2125
Email:jan.bogaert@ulb.ac.be

BIN TAN
Department of Geography, Boston University, Boston, MA 02215, USA
Tel: 617-353-1049
Fax: 617-353-8399
Email: tanbin@crsa.bu.edu

CURTIS E. WOODCOCK
Department of Geography, Boston University, Boston, MA 02215, USA
Tel: 617-353-5746
Fax: 617-353-8399
Email: curtis@bu.edu

YURI KNYAZIKHIN
Department of Geography, Boston University, Boston, MA 02215, USA
Tel: 617- 353-8843
Fax: 617- 353-8399
Email: jknjazi@crsa.bu.edu

RAMAKRISHNA R. NEMANI
Ecosystem Science and Technology Branch, NASA Ames Research Center, Moffett field, CA, 94035
Tel: 650-604-6185
Fax: 650-604-4680
Email: nemani@ntsg.umt.edu

RANGA B. MYNENI
Department of Geography, Boston University, Boston, MA 02215, USA
Tel: 617- 353-5742
Fax: 617- 353-8399
Email: rmyneni@crsa.bu.edu

Article Type (Review Article)

A rank based algorithm for aggregating land cover maps with minimal information loss

JIANNAN HU*§, JAN BOGAERT†, BIN TAN§, CURTIS E. WOODCOCK§,

YURI KNYAZIKHIN§, RAMAKRISHNA R. NEMANI‡, RANGA B. MYNENI§

§Department of Geography, Boston University, Boston, MA 02215, USA
†Université Libre de Bruxelles, École Interfacultaire de Bioingénieurs, Laboratoire d'Écologie du Paysage, Avenue F.D. Roosevelt 50, Bruxelles, Belgique

‡ Ecosystem Science and Technology Branch, NASA Ames Research Center, Moffett field, CA 94035, USA

Correspondence

Jiannan Hu

Department of Geography

Boston University

675 Commonwealth Avenue

Boston, MA 02215, USA

Telephone: 617-353-8845

Fax: 617-353-8399

Email: jiannan@crsa.bu.edu

Submitted for publication in
International Journal of Geographical Information Science
May 2005

A rank based algorithm for aggregating land cover data sets to coarser resolutions with minimal change in information content is presented in this paper. The method uses patterns in a fine resolution image to preferentially aggregate blocks that show homogeneity, majority and adjacency. Disappearance of classes is avoided by predefining the number of pixels of each class that should be present in the coarser resolution data set. The ranked aggregation algorithm is compared with two aggregation techniques − majority aggregation and random aggregation. The ranked aggregation method is shown to better conserve the information presented in the original image relative to the other algorithms using spatial pattern metrics quantifying class proportions, contagion, and fragmentation. Similarity metrics such as Euclidean distance and Czekanowski coefficient indicate images aggregated using ranked aggregation to be more similar to the original image than aggregation results from other techniques. Ranked aggregation is also shown to be associated with less unpredictability than its alternatives and the number of blocks assigned to a minority class is found to be negligible.

Keywords: Ranked aggregation algorithm; Map; Scale; Spatial pattern; Similarity; Class proportions; Contagion; Fragmentation; Euclidean distance; Czekanowski coefficient; Accuracy; Unpredictability

AMS Subject Classification: 86A32; 86A99

1. Introduction

The understanding and modeling of natural and anthropogenic processes which affect the Earth's environment require the production of land cover and land use maps at broad spatial scales (Mayaux and Lambin, 1995). For global scale research, data aggregation is primarily practiced for "scaling up" environmental analysis or models from local to landscape, regional, or global scales (Moody and Woodcock, 1996). Satellite data typically available at fine resolutions need to be coarsened to represent the spatial characteristics (spatial pattern, spatial autocorrelation, etc.) at scales used by global models.

The scale of data is associated with its resolution, which is defined as the area represented by one single pixel (DeMers, 1997), or more generally, as the degree to which small objects are distinguishable (Forman and Godron, 1986; Forman, 1997). The scale is often expressed in terms of grain and extent, describing the minimum spatial resolution of the data and the width of the study area, respectively (Milne, 1991; McGarigal and Marks, 1995; Hargis et al., 1998). The grain then determines the lower limit of what can be studied. Coarsening the spatial resolution leads to a loss of spatial details at a rate that depends on the spatial structure or heterogeneity of the landscape (Woodcock and Strahler, 1987; Townshend and Justice, 1988; Moody and Woodcock, 1994, 1995, 1996). Landscape patterns, as observed by digital images generated by remote sensing appear or disappear at different scales (Farina 1998). Rare land cover types are lost when resolution becomes coarser; patchy arrangements disappear more rapidly with decrease in the resolution than contagious ones (Turner et al., 1989). This phenomenon is usually more pronounced when

the elements composing the spatial pattern (e.g., patches) are scattered and are as small as or smaller than a pixel of the aggregated image. As a result, the use of coarse resolution images poses divergent problems in the estimation of cover type areas and the assessment of its accuracy.

Aggregating data to a coarser resolution is often preferred because certain spatial patterns will not be revealed until the data are displayed at a coarser scale (e.g. Seyfried and Wilcox, 1995). It is well recognized that any aggregation method may lose certain spatial details. However some methods retain statistical characteristics of the data better than others (Bian and Butler, 1999). A question then arises as to how these aggregation effects can be evaluated.

Aggregation reduces the number of pixels in the image for a fixed spatial extent. Each pixel consequently represents a larger area. This can alter the statistical and spatial characteristics of the data. Models that use aggregated data become scale-dependent, i.e., their predictions differ when input data of different resolutions are used (Bian and Butler, 1999). Although this effect is well-recognized by the GIS, remote sensing, and other science communities that use spatial information (e.g., Moody and Woodcock, 1994, 1995; Marceau and Hay 1999; Milne and Cohen 1999), there are very few papers on the effects caused by different aggregation techniques. Studies that require aggregation often employ the most convenient method without taking all the effects into account. This may jeopardize the integrity of studies as well as subsequent decision-making process.

The goal of this study is to develop and test an algorithm that generates coarse resolution land cover maps at continental scale but minimizes changes relative to the original image. A series of 1 km and coarser maps of North American land cover are

generated. The algorithm performance is quantified in terms of spatial metrics commonly used in landscape ecology. This approach has two justifications. First, it was reported that class spatial pattern influences information change during aggregation (Moody and Woodcock, 1994, 1995). Second, it is accepted that land cover pattern is related to landscape function, a central hypothesis of landscape ecology, known as the pattern/process paradigm (Coulson et al., 1999). Using spatial patterns, we can document precisely the way certain algorithms alter or conserve certain characteristics of the spatial information presented in the original image.

The objectives of this investigation are – (a) to develop a new spatial aggregation algorithm that represents fine resolution data at a coarser resolution with minimal information loss, and (b) to evaluate the new algorithm through comparison to the random aggregation algorithm and the most widely used majority aggregation algorithm; this evaluation is performed through spatial metrics and parameters describing the predictability and accuracy of the aggregation results.

2. Data set and methods

2.1 *MODIS land cover map*

The International Geopsphere-Biosphere Programme (IGBP) set of 17 land cover classes (Belward et al., 1999) are provided by the MODIS land cover product. Figure 1 shows an image of the Northern American data set used in this paper. Table 1 shows the percentage

of each class in the image. The water class dominates the image making up 68% of the total number of pixels. The areal percentage of other classes varies between 0.001% and 7%. The size of the image allows us to avoid rounding-up when aggregating it to 2, 4, 8, 16, 32, 64 and 128 km resolution consecutively or non-consecutively. The number of coarse pixels in each row and column as a function of the image resolution is given in table 2.

2.2 *Metrics to represent image information*

Characteristics of landscape patterns are usually expressed in terms of connectedness (e.g. contagion, fragmentation), diversity (e.g. Shannon diversity, Simpson index), and image heterogeneity (e.g., class area evenness). We examined how these characteristics change with resolution and algorithm by calculating a series of metrics that adequately reflect pattern features. The landscape pattern metrics selected for this study quantify the relative percentage of different land cover classes, their spatial adjacencies, and represent overall image properties. Most metrics used here are from landscape ecology.

Pattern differences between the aggregated images and the original 1 km data are expressed as

$$R = \frac{M_r - M_1}{M_1} \tag{1}$$

where M_r are the metrics of aggregated image at spatial resolution r and M_1 is that of original image at 1 km spatial resolution.

2.2.1 Metrics based on class proportions. The distribution of patterns and their areas are important characteristics of any image. Conservation of areas in the aggregation procedure is consequently a prerequisite to limit pattern change since pattern can be defined as spatial distribution of area. We use the concept of class area evenness to quantify the presence of classes relative to each other. The length of the Lorenz curve (L) is used to assess the degree of evenness (Lorenz 1905; Rousseau et al., 1999), which is calculated as follows. The class areas are replaced with relative values which are then ranked in ascending order. Let p_i ($p_i \geq p_{i-1}$) represents the relative area of *i*-th class and *z* be the total number of classes. The cumulative function of area distribution is given by

$$p_i^* = \sum_{j=1}^{i} p_j \tag{2}$$

The set of pairs (p_i^* , *i/z*), *i = 1*, *2*, …, *z*, is termed the Lorenz curve. To construct it, values of p_i^* are plotted on the ordinate against its rank number normalized by the total number of classes on the abscissa. The length of the Lorenz curve *L* can be calculated from the graph as (Bogaert et al., 2000b),

$$L = \sum_{i=1}^{z} \sqrt{\frac{1}{z^2} + \left(p_i^* - p_{i-1}^*\right)^2} = \sum_{i=1}^{z} \sqrt{\frac{1}{z^2} + \left(p_i\right)^2} \tag{3}$$

In case of perfect evenness, i.e. $\forall i, j \leq z : p_i = p_j$, the curve coincides with the diagonal (1:1 line) and $L = \sqrt{2}$. For a series in which a certain area dominates over others, $\exists i \neq j : p_i >> p_j, L \approx 2$. Evenness can be interpreted as a partial order (Rousseau et al., 1999) and thus adequately represented by a Lorenz curve (Taillie 1979).

Note that curves can cross each other in which case evenness can not be used for they can generate identical L values (Bogaert et al., 2000b). We use the Shannon (H_1) (Shannon and Weaver, 1949) and Simpson diversity (H_2) (Simpson 1949) indices to characterize the diversity of the classes. These are defined as

$$H_1 = -\sum_{i=1}^{z} p_i \ln(p_i) \tag{4}$$

$$H_2 = -\ln \sum_{i=1}^{z} p_i^2 \tag{5}$$

The higher their values the more diverse the image is. The diversity metrics depend on two variables – the richness component shows the number of classes present and the evenness component quantifies the distribution of the image pixels over the classes. The Shannon index is more sensitive to the richness component while the Simpson index is relatively less sensitive to richness and places more weight on the common classes (McGarigal and Marks 1995). These indices, therefore, can show considerable variation in response to changes in landscape richness and evenness.

The proportion estimation error (E_i) is used as a fourth descriptor. This metric shows whether an aggregation procedure results in an over- or underestimation of class areas. This variable is defined as (Moody and Woodcock, 1994)

$$E_i = \frac{p_{ci} - p_{fi}}{p_{fi}} \tag{6}$$

where p_{ci} and p_{fi} are relative areas of class *i* at the coarse and fine resolutions. An overall effect of the aggregation procedure of class proportion is given by the mean error over classes and its standard deviation.

2.2.2 Contagion metric. Contagion (*C*) measures the degree to which the image is composed of a few large or several small patches (O'Neill et al., 1988). It ranges between 0 and 1. High values indicate that the image is clumped into a few large patches. The metric accounts for adjacency and is expressed in terms of conditional probabilities $p_{i,j}$ of class *i* given that one of its neighboring pixels belongs to class $j (i \neq j)$ as

$$C = 1 + \frac{1}{2\ln(z)} \sum_{i=1}^{z} \sum_{j=1}^{z} p_{i,j} \ln(p_{i,j}) \tag{7}$$

where *z* is the number of classes in the image. Contagion measures both class interspersion (intermixing of classes) as well as class dispersion (the spatial distribution of the class). It is

one of the most frequently applied and commented landscape metrics in landscape ecology to characterize landscape pattern (e.g., Schumaker 1996; Hargis et al., 1998; O'Neill et al., 1999).

2.2.3 Monmonier fragmentation metric. Fragmentation describes the spatial scatter of pixels. Measurement of class fragmentation is still a subject of debate (Bogaert et al., 2002; Bogaert 2003) but a tendency towards simpler metrics quantifying components of complex spatial patterns was suggested (Giles and Trani, 1999). Therefore, a simple fragmentation metric (*F*) based on the grouping of adjacent pixels of the same class into patches is used in this study (Monmonier 1974; Johnsson 1995),

$$F = \frac{m_1 - 1}{m_2 - 1} \tag{8}$$

where m_1 and m_2 are numbers of patches and pixels, respectively. This metric varies between two extremes, 0 and 1. If all pixels are grouped into a single patch, $F = 0$. For maximum fragmentation, $m_1 = m_2$ and $F = 1$. To calculate *F*, aggregation of pixels into patches based on pixel neighborships for each class is required. Two pixels are grouped in one patch if they are orthogonal neighbors (nearest neighbors) and if they belong to the same class (Bogaert et al., 2000a). Orthogonal neighbors are also denoted as adjacent.

Patch mosaics constitute another level of structural composition of the image. Patches are treated as spatially homogeneous entities and relationships between patches can consequently be studied (Fortin 1999). The conversion of pixel-format into patch-format

data can be performed using standard software. We will calculate F two ways. First, equation (8) is calculated for the entire image. Second, we evaluate F for each class and then calculate the average over the classes.

2.2.4 Probability of adjacency. We measured the conditional probability of adjacency (p_c), that is, given a pixel of class of interest, the nearest neighbor is also a pixel of the class of interest (Riiters et al., 2000). This measure is considered an alternative assessment of fragmentation and is calculated as

$$p_c = \frac{n_2}{n_1} \tag{9}$$

with n_1 the number of pixel pairs that include at least one pixel of the class of interest and n_2 the number of pixel pairs of which both pixels belong to the class of interest. The measure p_c is calculated in a 3×3 template window. Diagonally adjacent pixels are not considered as pixel pairs. The measure p_c equals zero if none of the pairs includes pixels of interest; p_c equals one if all pixels in the template are pixels of the class of interest. The average probability per class can be determined using the distribution of the template values.

2.2.5 Similarity metrics. We use similarity metrics to quantify changes in image as a function of resolution. Such metrics combine the information provided by every separate pattern component and express the extent to which the coarse resolution image is similar to

the original one. The Euclidean distance $ED_{i,j}$, between two images *i* and *j*, is denoted as

$$ED_{i,j} = \sqrt{\sum_{m=1}^{n} (x_{m,i} - x_{m,j})^2} \tag{10}$$

where $x_{m,i}$ and $x_{m,j}$ are the metrics values, observed in images *i* and *j*, respectively. The larger $ED_{i,j}$ is, the less similar two images are. The Euclidean distance is the length of the distance between two images by accounting for the 7 metrics we calculated. For *F*, the average class data were used to determine similarity. A second similarity index known as the Czekanowski coefficient (Motyka et al., 1950; Legendre et al., 1979) expresses the percentage of similarity ($PS_{i,j}$) between two images and is calculated as

$$PS_{i,j} = \left(\frac{2w}{t+r} \right) \times 100 \tag{11}$$

Here *w*, *t* and *r* are

$$w = \sum_{m=1}^{n} \min(x_{m,i}, x_{m,j}) \tag{12}$$

$$t = \sum_{m=1}^{n} x_{m,i} \text{ and } r = \sum_{m=1}^{n} x_{m,j} \tag{13}$$

For two identical images, $PS_{i,j} = 100\%$.

2.2.6 Accuracy metric. Accuracy assessment is used to quantify product quality. We applied accuracy assessment in evaluating coarse landcover maps aggregated by different aggregation algorithms and different approaches (consecutive and non-consecutive). For a given land cover map, factors such as resolution, aggregation algorithm, and approach can affect accuracy. The reference data used in the accuracy assessment is the 1km IGBP land cover map. In this paper, aggregation accuracy is defined as the average percent fraction of labeled class of all pixels in the original 1km IGBP landcover map,

$$ACCU = \frac{\sum_{i=1}^{n} p_i}{n} \tag{14}$$

For a specified aggregated map, n is the total pixel number, p_i is the accuracy of pixel i. For example, consider an aggregated 2km coarse-resolution map and a pixel labeled as "grassland". Let 3 out of the 4 subpixels in the 1km map belong to the grassland class and one subpixel is labeled "savanna". The accuracy of the pixel in the 2 km image is then given by the proportion of the subpixel numbers that belong to the same class as the pixel in the coarse resolution image, i.e., 3/4 = 0.75. It should be noted that different aggregation algorithms and approaches could have different classes at the coarse resolution and thus have different accuracy values. In this case, aggregation accuracy reflects the agreement between coarse resolution class and subpixel land cover in the original IGBP map (Latifovica and Olthof, 2004).

2.3 *Aggregation algorithms*

Numerous aggregation methods have been reported in remote sensing literature. The most widely used procedures are averaging over all pixels, nearest neighbor resampling, or choosing the dominant value (Turner 1989; Bian 1997; Gardner 1998). In the following description, we denote pixels of the original image as "subpixels", and the aggregated coarse resolution pixels as the "pixels". The aggregation window (in the following sections is always a 2×2 subpixel window) is denoted as a "block". Figure 2 shows the algorithms considered in this study. Only non-overlapping blocks are considered in this study. For random and majority aggregations, both consecutive and non-consecutive approaches are used. In the non-consecutive approach, every coarse image is aggregated from the original 1km image directly. In the consecutive approach, a fixed aggregation window of 2×2 subpixels is used, which means that an image with resolution z serves as the input for an image with resolution $2z$.

2.3.1 Majority aggregation. This is the most widely used aggregation procedure. It uses a line by line scanning sequence, generally starting at the upper left corner of the image and ending at the bottom right corner, and every cluster of subpixels is aggregated independently. This technique attributes a pixel to a class based on the dominant subpixel class in the block. If several classes are present with the same fraction, a random class selection is made. The number of blocks with randomly selected classes will account for uncertainty or lack of predictability in the aggregated images (figure 2). This algorithm is

not area-conservative, i.e., classes that have large contiguous patches will stay in the aggregated image while classes showing scattered small patches may disappear. This characteristic should be avoided.

2.3.2 Random aggregation. With random aggregation, the image is aggregated line-by-line and every aggregation action is independent of the preceding actions. A random selection is made among the subpixels in the block. Classes with majority patterns will be favored due to an enhanced probability of being selected. Nevertheless, this does not exclude the assignment of pixels to a class that was dominated by another one in the block. With this approach, and except for homogeneous patterns in which all four subpixels belong to the same class, every aggregation step involves a random selection. The initial proportions of the classes are likely to be conserved due to this randomization effect (Gardner 1998). This will decrease the degree of predictability of the aggregated map product which may be considered as a negative characteristic of this technique.

2.3.3 Ranked aggregation. A new aggregation procedure is proposed which is more conservative with regard to class area and spatial pattern, that is, the proportional area of every class in the aggregated image remains similar to that in the original image. Metrics describing the spatial pattern in the original image are conserved maximally. In the proposed algorithm, the original image is not scanned line by line, but crisscross movements across the image are made. Some blocks are preferentially aggregated. This irregular selection of blocks is governed by well-defined rules given below. Aggregation of subpixels into pixels are not independent events, i.e., the aggregation result of the *i*-th block

is determined by earlier aggregations, e.g., the $(i-1)$th pixel, in the same image. Blocks could be assigned to the minority class instead of the dominant class. These two features constitute the main difference of this new algorithm.

Consider an image $I_{m\times m}$ with $m\times m$ subpixels. This image is aggregated using 2×2 non-overlapping aggregation windows or blocks into $I_{n\times n}$, with $n=m/2$. Every 4 subpixels in $I_{m\times m}$ are replaced by one single pixel in $I_{n\times n}$. Consider *z* classes in $I_{m\times m}$ of areas $a_1, a_2, \ldots, a_z$. Given class *j*, the a_j subpixels exhibit a particular spatial pattern in $I_{m\times m}$; if the blocks are superimposed on the original image, 10 different block types can be observed (figure 3):

(1) Blocks composed of 4 subpixels of class *j* and denoted as {4, 0, 0, 0}. This is a homogeneous block type with complete dominance of class *j*.

(2) Blocks containing 3 subpixels of class *j* and one subpixel from another class denoted as {3, 1, 0, 0}. This is a heterogeneous block type with dominance of class *j*.

(3) Blocks containing 2 adjacent subpixels of class *j* next to 2 subpixels from two other classes with notation $\{2, 1, 1, 0\}_a$. This is a heterogeneous block type with dominance of class *j*.

(4) Blocks containing 2 diagonally placed subpixels of class *j* and 2 subpixels from two other classes with block type notation $\{2, 1, 1, 0\}_d$. This is a heterogeneous block type with dominance of class *j*.

(5) Blocks containing 2 adjacent subpixels of class *j* and 2 adjacent subpixels from another class denoted as $\{2, 2, 0, 0\}_a$. This is a heterogeneous block type with evenness between the 2 classes presented.

(6) Blocks containing 2 diagonally placed subpixels of class *j* next to 2 diagonally placed

subpixels from another class which is denoted as $\{2, 2, 0, 0\}_d$. This is a heterogeneous block type with evenness between the 2 classes presented.

(7) Blocks containing 4 subpixels from 4 different classes which is denoted as $\{1, 1, 1, 1\}$. This is a heterogeneous block type with evenness between the 4 classes presented.

(8) Blocks containing 1 subpixel of class j and 3 subpixels from two other classes. If the two subpixels belonging to the same class are diagonally placed this block type is denoted as $\{1, 1, 2, 0\}_d$. This is a heterogeneous block type in which class j is dominated by another class.

(9) Blocks containing 1 class j subpixel next to 3 subpixels from two other classes. If the two subpixels belonging to the same class are adjacent this block type is denoted as $\{1, 1, 2, 0\}_a$. This is a heterogeneous block type in which class j is dominated by another class.

(10) Blocks containing 1 subpixel of class j next to 3 subpixels from another class which is denoted as $\{1, 3, 0, 0\}$. This is a heterogeneous block type in which class j is dominated by another class.

Consider the areas of the z classes in the aggregated image, i.e., $a'_1, a'_2, \ldots, a'_z$. In the ideal case, the relationship between a_j and a'_j is then given by

$$a_j = 4a'_j \tag{15}$$

Let $N^j_{BlockType}$ be the number of blocks of a particular type of class j with "$_{BlockType}$" the block type notation. A remotely sensed image of a landscape exhibits hierarchical patterns. It can

be accepted that generally $N^j_{\{4,0,0,0\}}$ and $N^j_{\{3,1,0,0\}}$ will compose the majority class pattern features of class *j*, while, for example, $N^j_{\{1,1,1,1\}}$, $N^j_{\{1,1,2,0\}d}$ and $N^j_{\{1,3,0,0\}}$ will form the minority class pattern components.

The starting point in the aggregation procedures is, first, all $N^j_{\{4,0,0,0\}}$ block types are aggregated. By doing this, a part of the a'_j pixels are already specified. Pixel assignment of the $N^j_{\{4,0,0,0\}}$ blocks does not involve any information loss because of the homogeneity of the pixels. The total area of pixels generated in this way is denoted as α'_j, and is related to a'_j as

$$a'_j = \alpha'_j + \beta'_j \tag{16}$$

with β'_j class *j* pixels in the aggregated image that result from heterogeneous blocks without loss. It should be noted that generally $a'_j > \alpha'_j$. Only if $\beta'_j = 0$, the aggregation procedure is complete after this initial step which is executed first for all *z* classes. It can even be concluded that the original map contained redundant information by presenting the data at a resolution finer than required when $\beta'_j = 0$. After this step, $4\sum_{i=1}^{k} N^i_{\{4,0,0,0\}}$ subpixels are aggregated.

All remaining pixels have to be assigned for every class except for the case of $\beta'_j = 0$. These pixels have to be selected from those blocks containing at least one single pixel of class *j*. The aggregation at each step is based on the ranking of the block types:

$$\{3,1,0,0\} \rightarrow \{2,1,1,0\}_a \rightarrow \{2,1,1,0\}_d \rightarrow \{2,2,0,0\}_a \rightarrow \{2,2,0,0\}_d$$
$$\rightarrow \{1,1,1,1\} \rightarrow \{1,1,2,0\}_d \rightarrow \{1,1,2,0\}_a \rightarrow \{1,3,0,0\} \tag{17}$$

with $\rightarrow$ indicating the order of aggregation. Within a class all blocks of type $\{3,1,0,0\}$ have to be first aggregated followed by blocks types $\{2,1,1,0\}_a$, $\{2,1,1,0\}_d$, $\{2,2,0,0\}_a$, $\{2,2,0,0\}_d$, $\{1,1,1,1\}$, $\{1,1,2,0\}_d$, $\{1,1,2,0\}_a$, and $\{1,3,0,0\}$. This is repeated until β'_j blocks are aggregated. If different blocks of a certain pattern type are present in the $I_{m\times m}$ image, for example, in the initial phase of the aggregation, a random selection is made among them.

The rank in equation (17) is based on the principles of "subpixel majority" and "subpixel connectivity". In the heterogeneous blocks with type $\{3,1,0,0\}$, $\{2,1,1,0\}_a$ and $\{2,1,1,0\}_d$, class j is dominant, with the latter two showing less dominance than the first. In configurations $\{2,2,0,0\}_a$, $\{2,2,0,0\}_d$ and $\{1,1,1,1\}$, none of the classes dominate, but the former two configurations have a higher priority because more subpixels of the class of interest are present. In $\{1,1,2,0\}_a$, $\{1,1,2,0\}_d$ and $\{1,3,0,0\}$, class j is dominated by other classes, but the dominance in configurations $\{1,1,2,0\}_a$ and $\{1,1,2,0\}_d$ is less pronounced than in $\{1,3,0,0\}$. The principle of connectivity indicates that, in case of equality, $\{2,2,0,0\}_a$ prevails over $\{2,2,0,0\}_d$. When class j is dominant, $\{2,1,1,0\}_a$ types will be aggregated before $\{2,1,1,0\}_d$. The same principle explains why $\{1,1,2,0\}_d$ blocks are chosen, and if this type is not available any more for class j, type $\{1,1,2,0\}_a$ will be aggregated.

This procedure is not executed class by class. Subpixels of more than one class are replaced by only one class in the coarse pixel image in the case of aggregating a

heterogeneous block. If a class-by-class aggregation were executed, it is possible that when the last class had to be aggregated all the blocks containing subpixels of this class were already assigned to other classes with which they have these blocks in common. Therefore, to determine the sequence of block aggregation, a ratio is defined as

$$\gamma_j = \frac{(\beta'_j)_r}{(\zeta_j)_r} \tag{18}$$

with $(\beta'_j)_r$ the number of blocks to be assigned to class *j*, and $(\zeta_j)_r$ the number of remaining blocks containing a subpixel of class *j*. The subscript "*r*" indicates remaining, and both $(\beta'_j)_r$ and $(\zeta_j)_r$ have to be recalculated after a block is assigned to a particular class. Classes with low values of $(\zeta_j)_r$ have a higher probability that not enough blocks are available relative to the required number $(\beta'_j)_r$. Therefore, a class with the highest γ-values is aggregated first according to the above mentioned rule of rank (equation (18)). After this assignment, all γ values are recalculated, and the procedure repeated. A class with the lowest $(\zeta_j)_r$ is chosen in the case of equal of γ-values. This procedure hence avoids $(\beta'_j)_r > (\zeta_j)_r$. A random selection is made among the classes involved in the case of identical $(\zeta_j)_r$ values.

The novelty and added value of this aggregation technique are in equations (17) and (18). Equation (17) describes the rank of the block types, giving preference to those types that contain a majority of the class of interest and to pattern connectivity (adjacent patterns

prevail on diagonal and vice versa in the case where the class of interest is a minority). Equation (18) describes how this rank is optimized for all classes and avoids disappearance of classes due to their initial scattered pattern. Neither line by line sequence nor a class by class sequence is used when the image is aggregated. The selection to which class a block is assigned and where this block is located in the image is not fixed unlike the other techniques. Instead, it is determined only by the spatial pattern of all classes at each stage. The non-consecutive approach was unrealizable for the ranked aggregation technique due to exponentially increasing number of block type patterns for block with dimensions greater than 2.

3. Results and discussion

We investigate how the relative presence of classes changes with resolution as a first step towards assessing the algorithm performance. Four variables quantify these changes – the Shannon and Simpson indices which measure the diversity of proportions, the Lorenz Curve Length which characterizes the evenness of these proportions, and the proportional errors. Figure 4(a) shows the relative values of the Lorenz Curve Length compared to that in the original image. Ranked aggregation does not change evenness proportion up to a resolution level of 128 km. Changes can be clearly seen at 2 km resolution in the case of majority aggregation, which indicates the appearance of class dominance. For example, deciduous needleleaf forests, urban and built-up areas (data not shown) are not present anymore in the coarse resolution images. Majority aggregation will favor classes with a

large extent. Consequently, large classes extend and smaller ones disappear. The increasingly negative value of the metric signifies a decreasing length of the Lorenz curve with aggregation, reflecting more proportional evenness.

Non-consecutive random aggregation closely follows the tendency in ranked aggregation up to a resolution of 32 km and then shows a positive deviation which indicates less evenness at 64 km resolution. The other techniques do not provide better results. The diversity of total class area (figures. 4(b) and 4(c)) is clearly altered by aggregation in the case of random and majority algorithms. This is especially true of the majority algorithm; the deviation is large for both consecutive and non-consecutive approaches and appears already after the first aggregation (2 km level). Ranked aggregation conserves the diversity of the class areas almost perfectly for both diversity metrics, especially at coarse resolutions (32 to 128 km).

The proportional error expresses the extent to which the proportion of each class in the image changes with resolution (figure 4(d)). Both majority aggregation algorithms have bigger proportional errors than other aggregation techniques and the increasingly negative trend of the curve indicates smaller proportions with aggregation. However, since an average value is used to reflect the image information content and the sum of the proportions at every scale level has to equal unity, this trend indicates that certain classes will have a smaller proportion due to aggregation (12 out of 19 classes), while the others show an increase (3 classes) or an irregular trend (4 classes). Ranked aggregation is the most effective in conserving the relative proportion of every class. Random aggregation techniques generate patterns similar to the original image at fine to moderate resolutions (2 to 16 km).

Contagion expresses the extent to which pixels of different classes are adjacent. It quantifies interspersion of classes and combines two features – fragmentation of classes and their spatial mixing. Contagion is calculated for the entire image and therefore reflects a characteristic of the overall spatial pattern. Contagion is based on the determination of the probability that a certain class is neighboring another one and accounts for the size differences between classes. Nevertheless, small classes remain more sensitive to the disappearance of one single pixel than large ones, which will likely alter the observed probability considerably at coarse resolutions. Ranked aggregation conserves the degree of contagion almost perfectly, with a deviation not exceeding 1% at fine to moderate resolutions (figure 5). At coarser resolutions, majority aggregation, both in the consecutive and non-consecutive mode, performs better although the contagion for all techniques shows a clear trend deviating from the horizontal reference line of no change. Random aggregation clearly does not conserve contagion and the choice between a consecutive or a non-consecutive way of generating the image series has no impact. All three techniques show a decreasing trend for contagion indicating a tendency towards smaller patches which is due to the smaller number of pixels available to represent pattern information. It should be noted that contagion is based only on pixel counts regardless of the area represented by them. The difference between random aggregation and majority/ranked aggregation is likely due to the fact that the former does not account for spatial relationships between pixels while the latter techniques favor conservation of pixels that are spatially grouped.

Figure 6 shows evolution of the Monmonier fragmentation index F for the 19 classes pooled. Fragmentation is measured by expressing the number of patches observed relative to the number of pixels. F tends to zero in the absence of fragmentation while F values

equal to unity indicate patches composed of a single pixel only. A general tendency of increasing fragmentation is observed with aggregation. A nearly linear increase of the fragmentation metric is seen for random aggregation, which results from the presence of more singular pixels at coarse resolutions. Figure 6(a) suggests a steady change in the spatial pattern of all classes pooled. No clear influence of the choice of input data (non-consecutive versus consecutive aggregation) is observed. The difference between the original and aggregated images increases with every aggregation step reflecting an increase in patches of single pixel. This tendency is not observed for ranked aggregation and majority aggregation. Both ranked and majority aggregations show less deviation from the original image and the change is not continuously increasing at every aggregation level. Ranked aggregation must be preferred over majority aggregation for this specific image as the relative differences are smaller. The upward trend in both curves reflects the representation of larger number of single pixel patterns. It should be noted that the Monmonier fragmentation metric does not account for pixel area and is only based on pixel counts, like the contagion metric.

Figure 6(b) uses class-based data to evaluate pattern change due to aggregation. While for random aggregation the aggregated pattern becomes rapidly more fragmented relative to the starting image, majority and ranked aggregation show less deviation from the original pattern at coarser resolution, especially when standard errors are taken into account. Except at 64 and 128 km, ranked aggregation is the most conservative towards pattern as quantified here by its degree of fragmentation. It should be noted that data series based on different aggregation rules are not fully comparable, especially at coarse resolutions, due to class disappearance with majority aggregation. This general trend where majority and

ranked aggregation perform better than random aggregation with regard to fragmentation is partially confirmed by separate analysis of every class (details not presented for brevity).

The probability of adjacency expresses the probability that if a pixel belongs to a certain class, its neighbor also represents that class. This probability is a measure of spatial dispersion of pixels of a class (class fragmentation) and quantifies the spatial mixing and connectivity of the classes. An overall view on pattern change with changing resolution is obtained by expressing this pattern characteristic using the average of the probabilities observed for every class.

Figure 7 shows the evolution of the average probability of adjacency for the three aggregation techniques. Random aggregation (both consecutive and non-consecutive) influences class dispersion (lower probabilities in coarse resolution images) and large deviations (~50% for non-consecutive random aggregation) are observed at coarse resolution. Nevertheless, the value obtained by consecutive random aggregation is closest to the original for the first aggregation step (2 km), while the other techniques immediately report a deviation of greater than 8% relative to the probability of adjacency in the original image. The average probability of adjacency decreases more rapidly with decreasing resolution for random aggregation compared to the other techniques. This decreasing trend is a direct consequence of the fact that subpixel groups present at fine resolution are replaced by more isolated pixels at coarser resolutions. Consecutive majority aggregation conserves the probability more thoroughly at fine to moderate resolutions (2-32 km). Ranked aggregation is more reliable at coarse resolutions. Note that non-consecutive majority aggregation never performs better than the ranked technique. It should be noted that both consecutive majority and ranked aggregation have nearly coinciding curves for

the range 2 to 32 km, which is also observed for 12 out of 19 classes (data not shown).

We calculated (dis)similarity metrics to assess change in image information relative to the original image. These metrics summarize the results described in detail above. Figure 8(a) shows evolution of the Euclidean distance with decreasing resolution. All techniques show a partially upward trend indicating persistent information change with aggregation. This can hardly be avoided as less information units are available in the coarse resolution images to represent the pattern complexity present in the original image. This was already observed from the preceding metrics individually. Their separate effects are superimposed in these similarity metrics. Ranked aggregation has clearly the smallest Euclidean distances (~0.05) at every resolution up to a resolution of 64 km. For consecutive majority aggregation, the Euclidean distance exceeds the distance measured by ranked aggregation, and for the non-consecutive majority rule, the difference is even higher. Consecutive random aggregation takes an intermediate position between both techniques and changes almost linearly with decreasing resolution.

The Czekanowski coefficient expresses the degree of similarity between the original and the aggregated images (figure 8(b)). The decreasing trends therefore indicate an increasing degree of pattern difference between the images. Majority aggregation is clearly less pattern conservative than ranked aggregation. The latter does not show a distinct pattern change up to 64 km, and the drop observed at 128 km does not pass the ~95% level, which is remarkable after that many aggregation steps. Consecutive random aggregation takes an intermediate position between consecutive majority and ranked aggregation also for the Czekanowski coefficient, except at 32 km, where it performs worse than consecutive majority aggregation. The use of non-consecutive approach does not enhance

the similarity between the high and low resolution images.

The results presented in figures. 4 to 8 express pattern changes with decreasing resolution which are indicative of algorithm performance. A complementary approach analyzes the decision processes of the various algorithms. When the predictability of the aggregation result is high and when the number of subpixels selected belonging to a minority class in the block is low, the aggregation result is more reliable, predictable, and closer to the information present in the original image. This tendency should be favored in developing aggregation algorithms.

Figure 9 shows the degree of unpredictability of the three aggregation algorithms. Unpredictability occurs when a class has to be selected randomly in the case of equal γ-values (equation (18)) for the ranked aggregation. Equal γ-values have only been observed for block type {3,1,0,0} during the aggregation. The associated unpredictability at every resolution is calculated as the ratio between the number of blocks randomly selected to the total number of blocks used to create the aggregated image (figure 9(a)). Low unpredictability levels (≤0.5%) are observed except at 64km. Nevertheless, the unpredictability (~ 1.5%) observed at this particular resolution is still relatively low. A higher degree of unpredictability is observed for the majority aggregation rule (figure 9(b)) and in particular for the consecutive mode, where the unpredictability ranges from 3.5% to 6 %. Unpredictability is introduced when the block types $\{2,2,0,0\}_a$, $\{2,2,0,0\}_d$, and {1,1,1,1} are present for this aggregation technique. Unpredictability is calculated as the ratio of the number these three block types to the total number of blocks. Note that unpredictability decreases sharply after the 4km resolution level for the non-consecutive approach. This is perhaps because class evenness in large aggregation blocks is improbable.

Non-consecutive random aggregation (figure 9(c)) generates the largest degree of unpredictability, which increases with decreasing resolution from ~15% to ~45%. Note that the consecutive approach generates less predicable results than its non-consecutive counterpart. Unpredictability is present in this aggregation algorithm every time when a heterogeneous block is encountered.

The number of subpixel minority classes to which a pixel is assigned is another indicator of algorithm performance. It is evident that this never occurs for majority aggregation. For ranked aggregation, the percentage of assigned minority classes, observed for block types $\{1,1,2,0\}_a$, $\{1,1,2,0\}_d$, and $\{1,3,0,0\}$, increases with resolution, but never passes the 0.2% level (figure 10), which means that it remains a marginal event.

The results of the accuracy assessment are presented in figure 11. All techniques show a decreasing trend indicating more subpixel heterogeneity. Majority aggregation performs slightly better than ranked aggregation but the tendencies are similar and the absolute differences between the curves are negligible. This is likely because both techniques favor pixel majority and adjacency. The marginally lower accuracy of the ranked aggregation technique is because it enables minority class assignment and conserves proportional class area at the same time. Random aggregation generates less accurate results as may be expected by its randomizing effect.

4. Conclusions

Multi-scalar land cover data are needed to model and quantify ecosystem processes at different spatial scales. This motivates the development of reliable aggregation algorithms which enable resolution coarsening with minimal information loss. We propose a new aggregation technique which maintains class evenness, diversity, proportion and patch diversity of the original image. The method uses spatial patterns in the fine resolution image as the starting point. Non-overlapping square-shaped aggregation windows or blocks containing four subpixels are parameterized in terms of adjacency, majority, and ambiguity which determine the type of the block. The blocks are then ranked with respect to their content. The frequency of the types per class determines the class to which a block is assigned to and the order in which blocks are processed. Well-defined rules to assign a class to the block minimize changes in the class proportions and overall characteristics of the original spatial patterns in the aggregated image. This is achieved by (i) aggregating homogeneous blocks which contains one single class, (ii) avoiding class disappearance through a step-by-step monitoring of subpixel loss per class (equation (18)), and (iii) giving aggregation preference to blocks showing majority and adjacency of subpixels. We used class proportion-based metrics in addition to image contagion and the Monmonier fragmentation metrics to characterize spatial patterns. We show that ranked aggregation technique better conserves the complex patterns in the original image. Some information changes are likely unavoidable as fewer pixels are available to represent information at coarser resolutions. Also, images generated with ranked aggregation are found to be more

similar to the original image than those created by random or majority aggregation. Our conclusions are confirmed by analyses of several predictability and accuracy parameters.

Acknowledgements

This research was funded by NASA Earth Science Enterprise. Financial support to Jan Bogaert by the FWO (contract 1.5.150.03), the FNRS (contract 1.5.028.05), and by the ULB (crédit extraordinaire de recherche) is gratefully acknowledged.

References

BIAN, L., 1997, Multiscale nature of spatial data in scaling up environmental models. In *Scale in Remote Sensing and GIS,* Quattrochi, D. and Goodchild, M. F. (Eds.). (Boca Raton, FL. CRC/Lewis Publishers).

BIAN, L. and BUTLER, R., 1999, Comparing effects of aggregation methods on statistical and spatial properties of simulated spatial data. *Photogrammetric Engineering and Remote Sensing*, **65(1)**, pp. 73–84.

BELWARD, A. S., ESTES, J. E., and KLINE , K. D., 1999, The IGBP-DIS global 1-km land-cover data set DISCover: a project overview. *Photogrammetric Engineering and Remote Sensing*, **65**, pp. 1013–1020.

BOGAERT, J., ROUSSEAU , R., VAN HECKE, P., and IMPENS, I., 2000a, Alternative area-perimeter relations for measurement of 2-D shape compactness of habitats. *Applied Mathematics and Computation*, **111**, pp. 71–85.

BOGAERT, J., ROUSSEAU, R., VAN HECKE, P., SALVADOR-VAN EYSENRODE, D. and CEULEMANS, R., 2000b, The Lorenz curve as an indicator of scale effect on image information content. In *Quantitative Approaches to Landscape Ecology*, Clare, T. and Howard, D. (Eds.), pp. 121–129, (IALE(UK), Bangor, UK).

BOGAERT J., VAN HECKE, P., and CEULEMANS, R., 2002, The Euler number as an index of spatial integrity of landscapes: evaluation and proposed improvement. *Environmental Management*, **29(5)**, pp. 673–682.

BOGAERT J., 2003, Lack of agreement on fragmentation metrics blurs correspondence between fragmentation experiments and predicted effects. *Conservation Ecology*, **7(1)**, r6.

COULSON, R. N., MCFADDEN, B. A., PULLEY, P. E., LOVELADY, C. N., FITZGERALD, J. W., and Jack, S. B., 1999, Heterogeneity of forest landscapes and the distribution and abundance of the southern pine beetle. *Forest Ecology and Management,* **114**, pp. 471–485.

DEMERS, M. N., 1997, *Fundamentals of Geographic Information Systems*. John Wiley and Sons, New York.

FARINA, A., 1998, *Principles and Methods in Landscape Ecology*. Chapman and Hall, London.

FORMAN, R. T. T., 1997, *Land Mosaics: The Ecology of Landscapes and Regions*. Cambridge: Cambridge University Press.

FORMAN, R. T. T. and GODRON, M., 1986, *Landscape Ecology*. New York: John Wiley & Sons.

FORTIN, M. J., 1999, Spatial statistics in landscape ecology. In *Landscape Ecological Analysis: Issues and Applications,* J. M. KLOPATEK, and R. H. GARDNER, (Eds.), pp. 253–279, (New York: Springer- Verlag).

GARDNER, R.H., 1998, Pattern, process, and the analysis of spatial scales. In *Ecological scale: Theory and applications,* D. L. PETERSON and V. T. PARKER, (Eds.), pp. 17–34, (New York: Columbia University Press).

GILES, R. H., and TRANI, M. K., 1999, Key elements of landscape pattern measures. *Environmental Management*, **23**, pp. 477–481.

HARGIS, C. D., BISSONETTE, J. A., and DAVID, J. L., 1998, The behavior of landscape metrics commonly used in the study of habitat fragmentation. *Landscape Ecology*, **19**, pp. 167–186.

JOHNSSON, K., 1995, Fragmentation index as a region based GIS operator. *International Journal of Geographic Information Systems*, **9**, 211–220.

LATIFOVICA, L. and OLTHOF, I., 2004, Accuracy assessment using sub-pixel fractional error matrices of global land cover products derived from satellite data. *Remote Sensing of Environment,* **90**, pp. 153–165.

LEGENDRE, L. and LEGENDRE, P., 1979, *Écologie numérique: la structure des données écologiques,* Les Presses de l'Université de Quebec, Paris.

LORENZ, M. O., 1905, Methods of measuring concentration of wealth. *Journal of the American Statistical Association,* **9(90)**, pp. 209–219.

MARCEAU, D. J., and HAY, G. J., 1999, Scaling and Modeling in Forestry: Applications in Remote Sensing and GIS. *Canadian Journal of Remote Sensing,* **25(4)**, pp. 342–346.

MAYAUX, P., and LAMBIN, E., 1995, Estimation of tropical forest area from coarse spatial resolution data: a two-step correction function for proportional errors due to spatial aggregation. *Remote Sensing of Environment,* **53**, pp. 1–15.

MCGARIGAL, K., and MARKS, B. J., 1995, *Fragstats: Spatial pattern analysis program for quantifying landscape structure*, Gen. Tech. Rep. PNW-GTR-351, USDA Forest Service, pp122, (Pacific Northwest Research Station, Portland, OR).

MILNE, B. T., 1991, Lessons from applying fractal models to landscape patterns. In *Quantitative Methods in Landscape Ecology*, M. G. Turner and R. H. Gardner, (Eds.), pp. 199–239, (Springer-Verlag, New York).

MILNE, B.T. and COHEN W. B., 1999, Multiscale assessment of binary and continuous landcover variables for MODIS validation, mapping, and modeling applications. *Remote Sensing of Environment* **70**, pp. 82–98.

MONMONIER, M.S., 1974, Measures of pattern complexity for choroplethic maps. *The American Cartographer*, **1(2)**, 159–169.

MOODY, A. and WOODCOCK, C.E., 1994, Scale-dependent errors in the estimation of land-cover proportions −implications for global land-cover datasets. *Photogrammetric Engineering and Remote Sensing*, **60**, pp. 585–594.

MOODY, A. and WOODCOCK C.E., 1995, The influence of scale and the spatial characteristics of landscapes on land-cover mapping using remote sensing. *Landscape Ecology*, **10(6)**, pp. 363–379.

MOODY, A., and WOODCOCK, C.E., 1996, Calibration-based models for correction of area estimates derived from coarse resolution imagery. *Remote Sensing of Environment*, **58(3)**, pp. 225–241.

MOTYKA, J., DOBRZANSKI B., and ZAWADZKI, S., 1950, Preliminary studies on meadows in the southeast of the province Lublin. *Ann. Univ. Mariae. Curie-Sklodowska Sect. E: Agricultura* **5**, pp. 367–447.

O'NEILL, R. V., KRUMMEL, J. R., GARDNER, R. H., SUGIHARA, G., JACKSON, B., DEANGELIS, D. L., MILNE, B. T., TURNER M. G., ZYGMUNT, B.,

CHRISTENSEN, S. W., DALE, V. H., and GRAHAM, R. L., 1988, Indices of landscape pattern. *Landscape Ecology*, **3**, pp. 153–162.

O' NEILL, R. V., RIITERS, K. H., WICKHAM, J. D., and JONES, K. B., 1999, Landscape pattern metrics and regional assessment. *Ecosystem Health*, **5**, pp. 225–233.

RIITERS, K. H., WICKHAM , J. D., O' NEILL, R. V., JONES, K. B., and SMITH, E., 2000, Global-scale patterns of forest fragmentation. *Conservation Ecology*, **4(1)**, pp. 3.

ROUSSEAU, R., VAN HECKE, P., NIJSSEN, D., and BOGAERT, J., 1999, The relationship between diversity profiles, evenness and species richness based on partial ordering. *Environmental and Ecological Statistics*, **6(2)**, pp. 211–223.

SCHUMAKER, N. H., 1996, Using landscape indices to predict habitat connectivity. *Ecology*, **77**, pp. 1210–1225.

SEYFRIED, M. S., and WILCOX, B. P., 1995, Scale and the nature of spatial variability: field examples having implications for hydrologic modeling. *Water Resources Research,* **31**, pp. 173–183.

SHANNON, C. E. and WEAVER, W., 1949, *The Mathematical Theory of Communication*. Urbana, IL: The University of Illinois Press.

Simpson, E. H., 1949, Measurement of diversity. *Nature,* **163**, pp. 688.

TAILLIE, C. 1979, Species equitability: a comparative approach. In *Ecological Diversity in Theory and Practice,* J. F GRASSLE, G. P. PATIL, W. SMITH, and C. TAILLIE, (Eds.), pp. 51–65, (Fairland, MD: International Cooperative Publishing House).

TOWNSHEND, J. R. and JUSTICE, C.O., 1988, Selecting the spatial resolution of satellite sensors required for global monitoring of land transformations. *International Journal of Remote Sensing,* **9(2)**, pp. 187–236.

TURNER, M.G., O'NEILL, R.V., GARDNER, R.H., and MILNE, B.T., 1989, Effects of changing scale on the analysis of landscape pattern. *Landscape Ecology*, **3**, pp. 153–162.

WOODCOCK, C.E. and STRAHLER, A.H., 1987, The factor of scale in remote sensing. *Remote Sensing of Environment*, **21**, pp. 311–325.

Class	Coverage (%)
Water	68.073
Evergreen broadleaf forest	2.201
Evergreen needleleaf forest	4.026
Deciduous needleleaf forest	0.045
Deciduous broadleaf forest	1.086
Mixed forests	2.723
Closed shrublands	0.249
Open shrublands	7.546
Woody Savannas	1.772
Savannas	0.758
Grasslands	2.697
Permanent wetlands	0.172
Croplands	2.895
Urban and built-up	0.112
Cropland/Natural vegetation mosaic	1.201
Snow and ice	2.81
Barren or sparsely vegetated	1.437
Unclassified	0.197
Fill value	0.001

Table 1

Coverage of the 17 International Geosphere-Biosphere Programme (IGBP) classes in the North American data set shown in Figure 1.

Spatial resolution (km)	Rows	Columns
1 (IGBP original image)	8960	9216
2	4480	4608
4	2240	2304
8	1120	1152
16	560	576
32	280	288
64	140	144
128	70	72

Table 2

Images used to evaluate the aggregation procedures. The original image is the MODIS land cover map, i.e. the 8960×9260 pixel image with a spatial resolution of 1 km. This image serves as the input to the 2 km image, which is generated using a 2×2 window.

Figure captions

Figure 1. MODIS land cover image for North America, composed of 8996 rows and 9223 columns, at 1 km resolution in Lambert Azimutal equal area projection. The central meridian is located at 100 W and the central parallel at 50 N.

Figure 2. Illustration of the algorithms used in this paper. In (a) the original image (4×4) is given, composed of 16 subpixels and 4 classes. This image will be aggregated into an image with 2×2 pixels. In (b) the image resulting from majority aggregation is shown. The pixels correspond to classes represented by a majority of subpixels in the aggregation windows. In case of equity (e.g. presence of two biomes with two subpixels or presence of four biomes), a random selection is made. In this example, this random selection for the bottom right aggregation window can result in four different results. The image is aggregated line by line, starting in the upper left position of the image. In (c), the image created by random aggregation is given. The classes of the pixels are determined by a random selection among the subpixels in each aggregation window. Note that due to this random selection, 24 different results can be generated. Also random aggregation uses a line-by-line aggregation sequence. In (d), the result using the ranked aggregation algorithm is shown. The sequence of the aggregation is given in (e), hence no line-by-line aggregation is observed. Only one random selection (between the two classes represented by a hatched fill pattern) was needed during the application of the latter technique, to determine the last pixel class, which implies a higher predictability as compared to the other techniques. The reader will notice that the

aggregation results shown in (d) is the closest to the original set shown in (a) from visual perception, and that is the only case has one of the classes represented by striped pattern.

Figure 3. Illustration of the 10 block types and the notation for the ranked aggregation algorithm. The class represented by the black pixel is the class of interest. Pattern (a) is denoted as homogeneous, while the others are heterogeneous. In patterns (a) − (d), the selected subpixel has a majority in the aggregation window, while in patterns (h) − (j) the selected subpixel belongs to the minority in the block. In patterns (e) − (g), none of the classes is dominant. The "a", and "d" labels indicate that subpixels of the class of interest are adjacent and diagonally placed respectively. The numbers represent the subpixel number for each class.

Figure 4. Influence of spatial aggregation technique on class proportions. (a) Evenness assessment by means of the Lorenz curve length. (b) Proportion diversity assessment using the Shannon diversity index. (c) Proportion diversity assessment using the Simpson diversity index. (d) Assessment of the average deviation of every class proportion relative to the proportion in the original image by means of proportional error.

Figure 5. Influence of spatial aggregation on image contagion.

Figure 6. Influence of spatial aggregation on class fragmentation by means of the Monmonier Fragmentation metric. (a) Fragmentation assessment of all classes pooled. (b)

Assessment of the average class fragmentation relative to the degree of average fragmentation in the original image.

Figure 7. Influence of spatial aggregation on the mean probability of adjacency.

Figure 8. Analysis of pattern change due to spatial aggregation using similarity metrics. (a) Image pattern difference assessment using the Euclidean distance. (b) Image pattern difference assessment using the Czekanowski coefficient.

Figure 9. Assessment of unpredictability to illustrate algorithm performance. (a) Ranked aggregation − unpredictability is caused by the presence of random selections between classes due to equal γ-values. (b) Majority aggregation − unpredictability is caused by the presence of $\{2,2,0,0\}_a$, $\{2,2,0,0\}_d$, or $\{1,1,1,1\}$ block types. (c) Random aggregation − unpredictability is present in case of the heterogeneous block types.

Figure 10. Block assignment to a minority class as a parameter of algorithm performance. Minority assignment is observed for block types $\{1,1,2,0\}_a$, $\{1,1,2,0\}_d$, and $\{1,3,0,0\}$.

Figure 11. Accuracy of images aggregated using various aggregation algorithms.

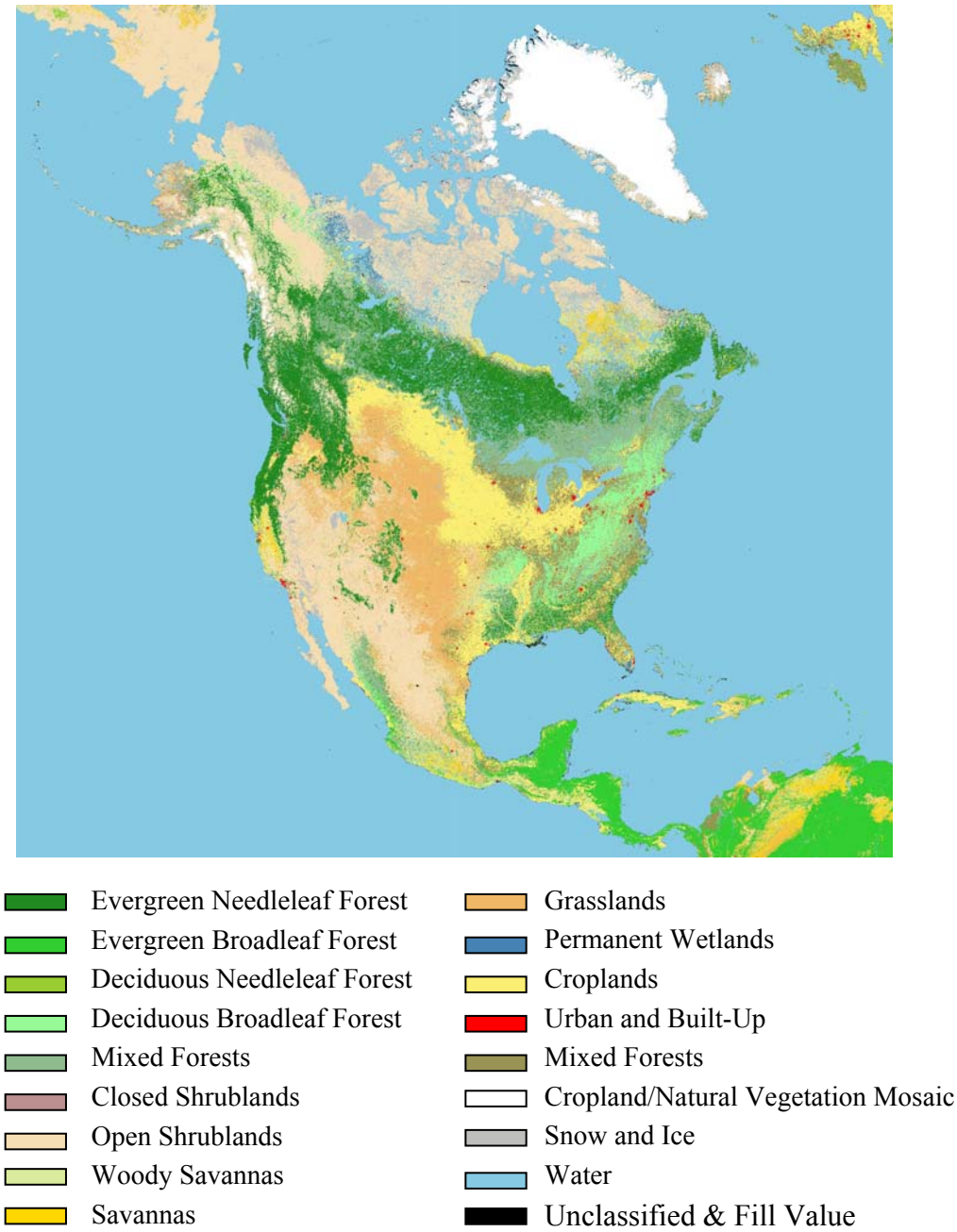

Figure 1. MODIS land cover image for North America, composed of 8996 rows and 9223 columns, at 1 km resolution in Lambert Azimutal equal area projection. The central meridian is located at 100 W and the central parallel at 50 N.

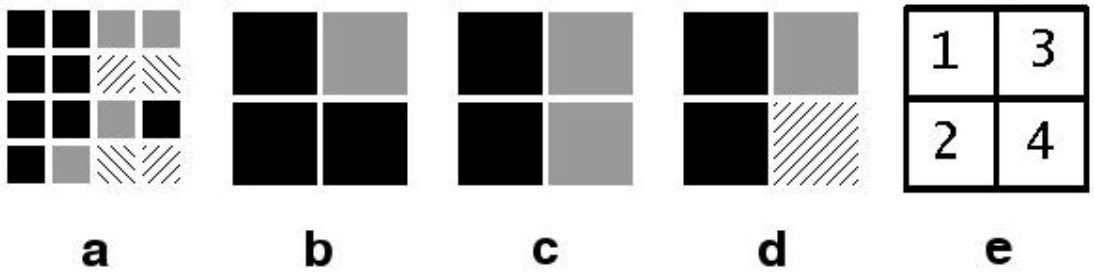

Figure 2. Illustration of the algorithms used in this paper. In (a) the original image (4×4) is given, composed of 16 subpixels and 4 classes. This image will be aggregated into an image with 2×2 pixels. In (b) the image resulting from majority aggregation is shown. The pixels correspond to classes represented by a majority of subpixels in the aggregation windows. In case of equity (e.g. presence of two biomes with two subpixels or presence of four biomes), a random selection is made. In this example, this random selection for the bottom right aggregation window can result in four different results. The image is aggregated line by line, starting in the upper left position of the image. In (c), the image created by random aggregation is given. The classes of the pixels are determined by a random selection among the subpixels in each aggregation window. Note that due to this random selection, 24 different results can be generated. Also random aggregation uses a line-by-line aggregation sequence. In (d), the result using the ranked aggregation algorithm is shown. The sequence of the aggregation is given in (e), hence no line-by-line aggregation is observed. Only one random selection (between the two classes represented by a hatched fill pattern) was needed during the application of the latter technique, to determine the last pixel class, which implies a higher predictability as compared to the other techniques. The reader will notice that the aggregation results shown in (d) is the closest to the original set shown in (a) from visual perception, and that is the only case has one of the classes represented by striped pattern.

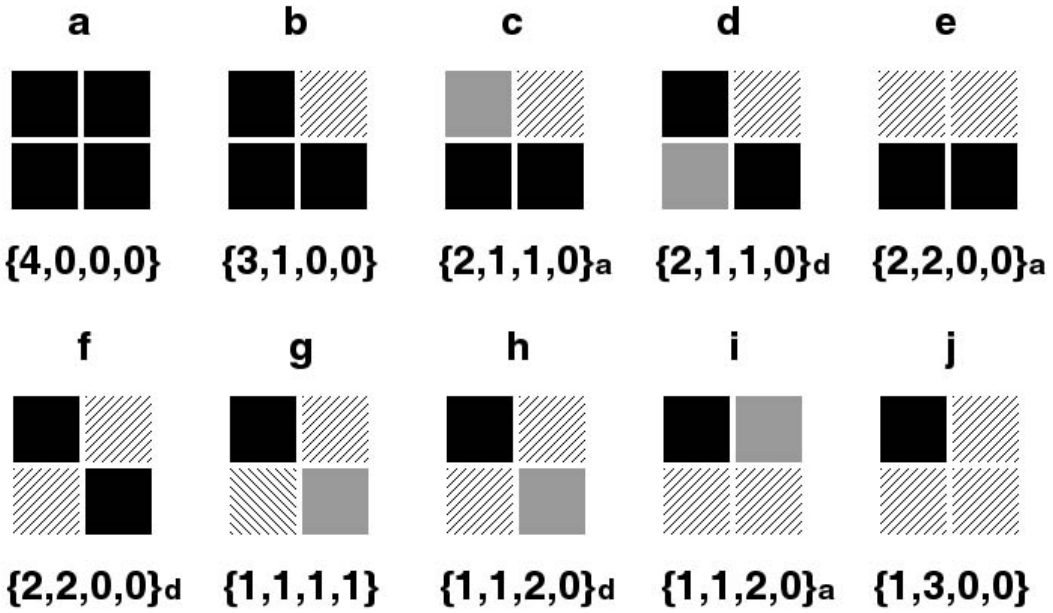

Figure 3. Illustration of the 10 block types and the notation for the ranked aggregation algorithm. The class represented by the black pixel is the class of interest. Pattern (a) is denoted as homogeneous, while the others are heterogeneous. In patterns (a) − (d), the selected subpixel has a majority in the aggregation window, while in patterns (h) − (j) the selected subpixel belongs to the minority in the block. In patterns (e) − (g), none of the classes is dominant. The "a", and "d" labels indicate that subpixels of the class of interest are adjacent and diagonally placed respectively. The numbers represent the subpixel number for each class.

(a)

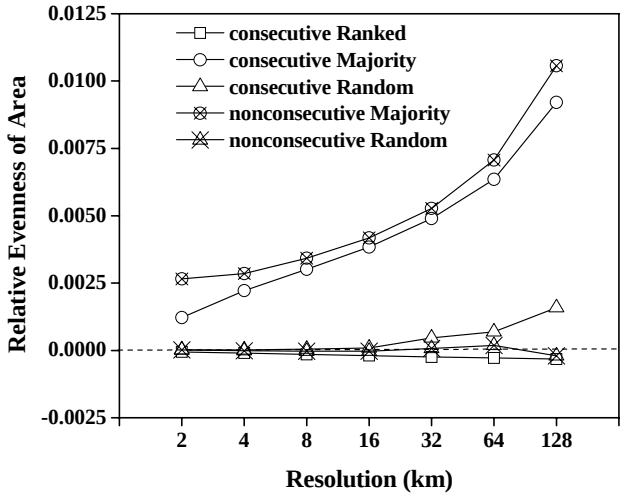
0.0125
0.0100
0.0075
0.0050
0.0025
0.0000
-0.0025
Relative Evenness of Area
consecutive Ranked
consecutive Majority
consecutive Random
nonconsecutive Majority
nonconsecutive Random
2
4
8
16
32
64
128
Resolution (km)

(b)

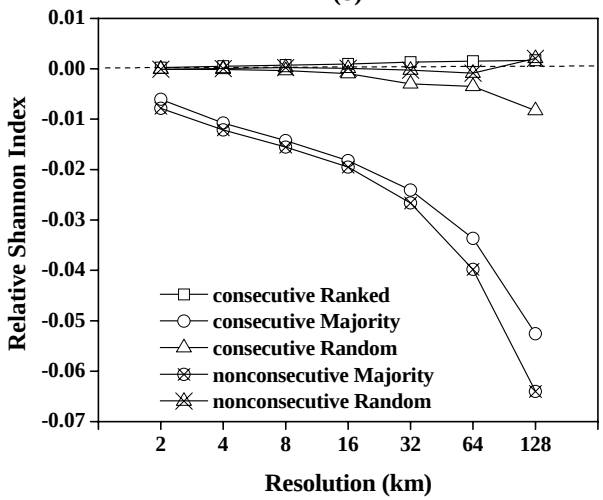
0.01
0.00
-0.01
-0.02
-0.03
-0.04
-0.05
-0.06
-0.07
Relative Shannon Index
consecutive Ranked
consecutive Majority
consecutive Random
nonconsecutive Majority
nonconsecutive Random
2
4
8
16
32
64
128
Resolution (km)

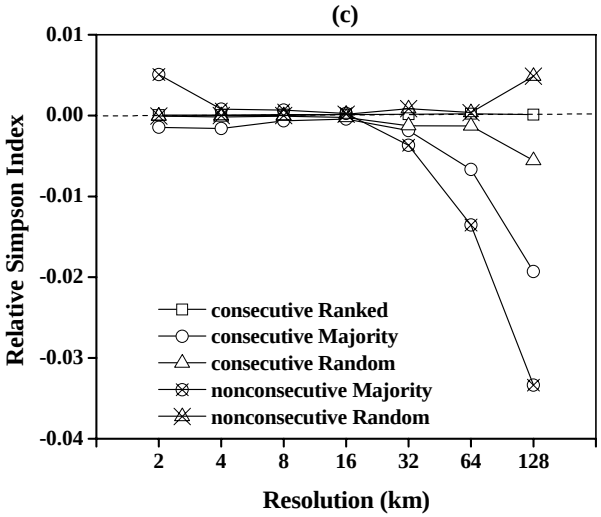

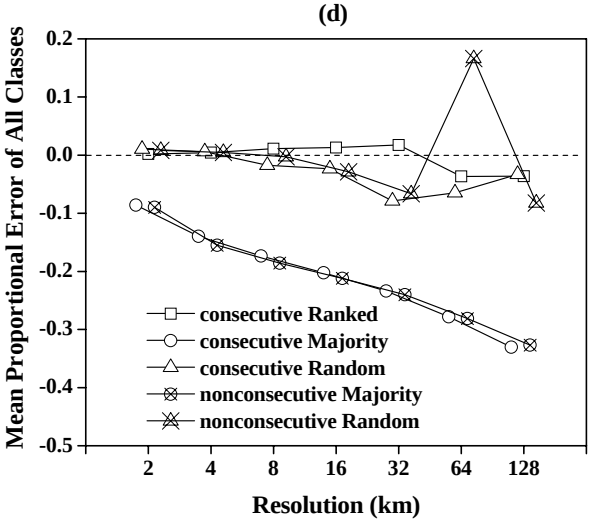

Figure 4. Influence of spatial aggregation technique on class proportions. (a) Evenness assessment by means of the Lorenz curve length. (b) Proportion diversity assessment using the Shannon diversity index. (c) Proportion diversity assessment using the Simpson diversity index. (d) Assessment of the average deviation of every class proportion relative to the proportion in the original image by means of proportional error.

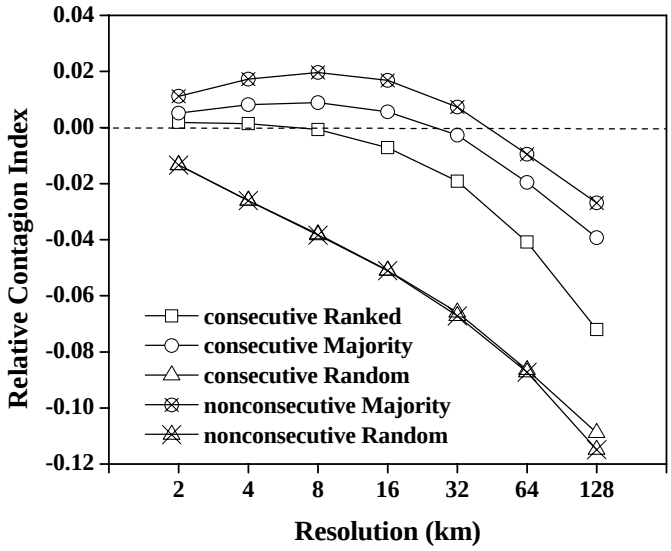

Figure 5. Influence of spatial aggregation on image contagion.

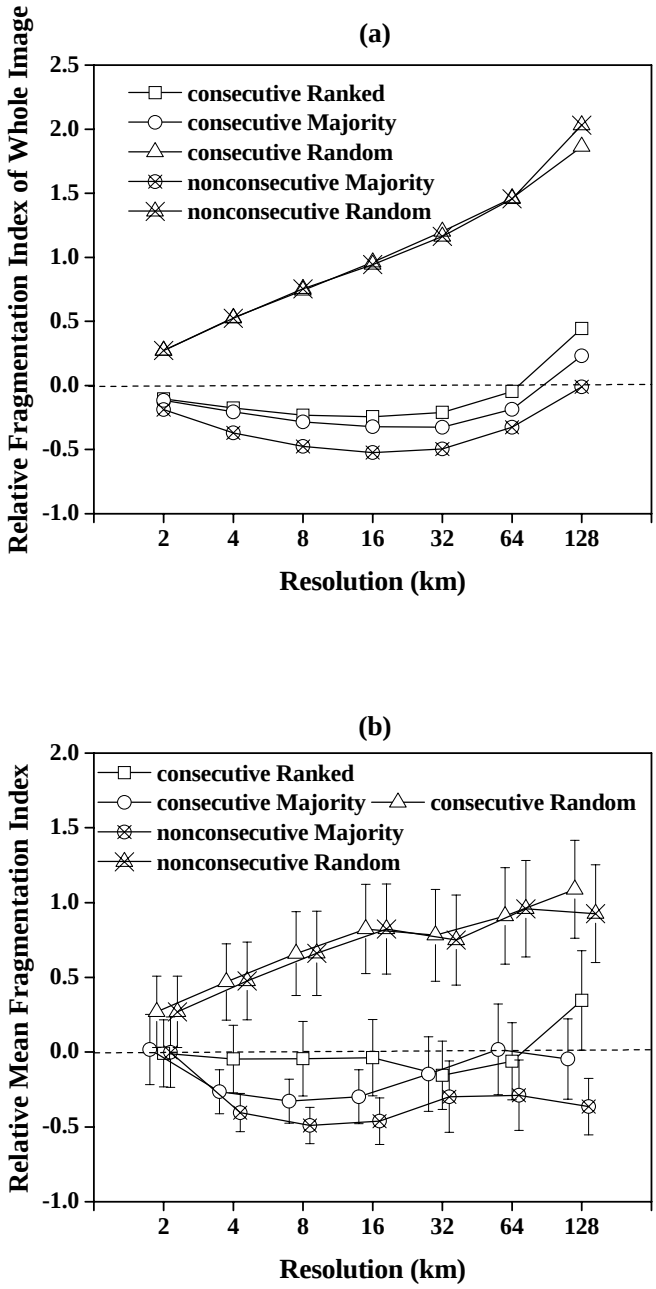

Figure 6. Influence of spatial aggregation on class fragmentation by means of the Monmonier Fragmentation metric. (a) Fragmentation assessment of all classes pooled. (b) Assessment of the average class fragmentation relative to the degree of average fragmentation in the original image.

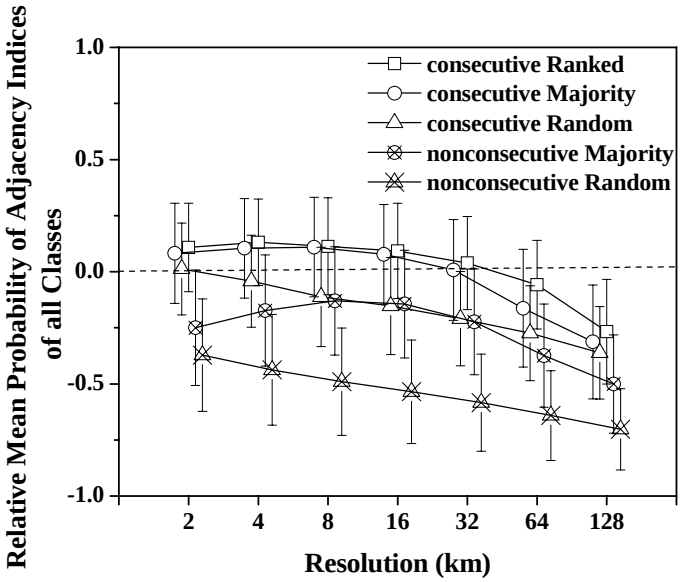

Figure 7. Influence of spatial aggregation on the mean probability of adjacency.

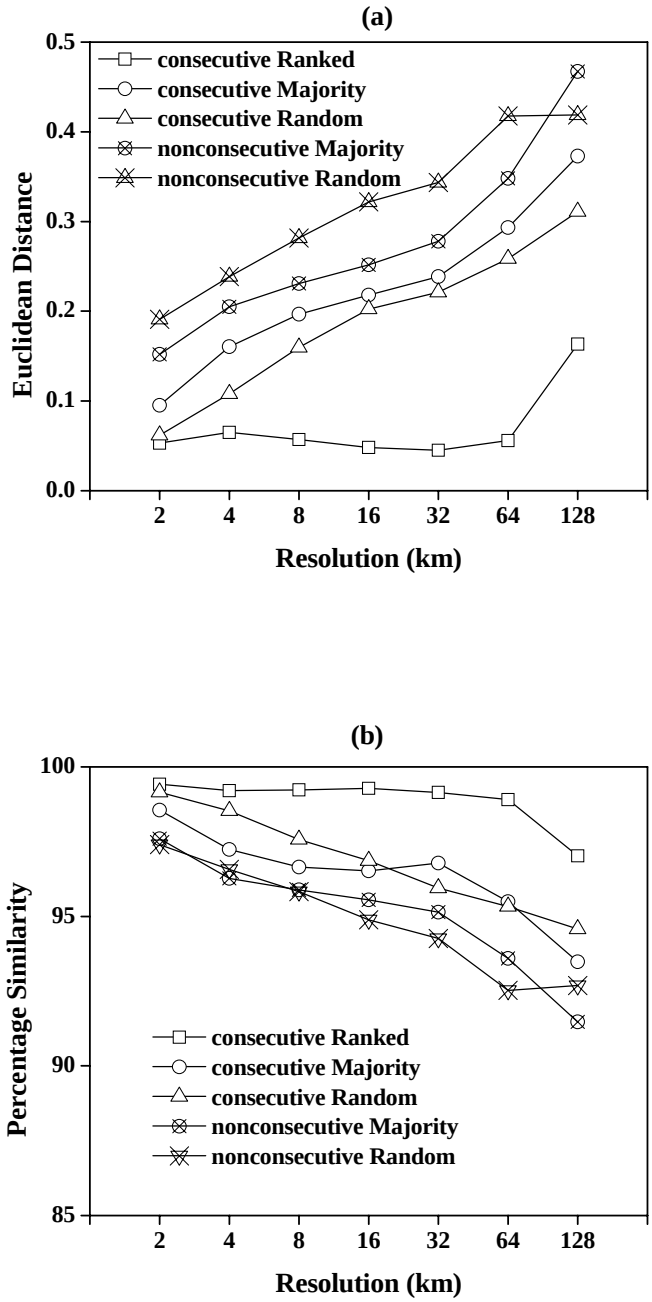

Figure 8. Analysis of pattern change due to spatial aggregation using similarity metrics. (a) Image pattern difference assessment using the Euclidean distance. (b) Image pattern difference assessment using the Czekanowski coefficient.

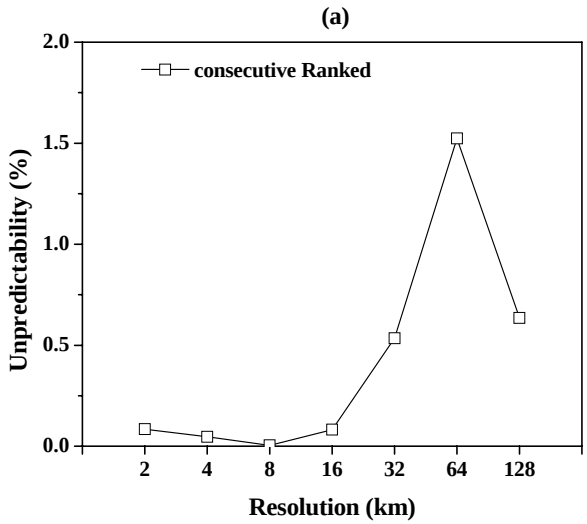
(a)
consecutive Ranked
Unpredictability (%)
2.0
1.5
1.0
0.5
0.0
2
4
8
16
32
64
128
Resolution (km)

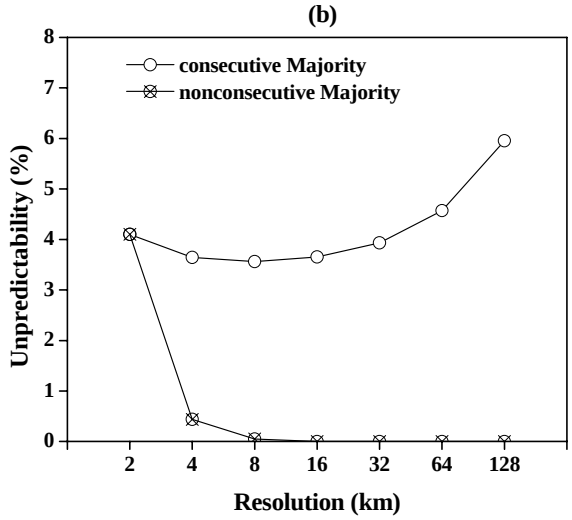
(b)
consecutive Majority
nonconsecutive Majority
Unpredictability (%)
8
7
6
5
4
3
2
1
0
2
4
8
16
32
64
128
Resolution (km)

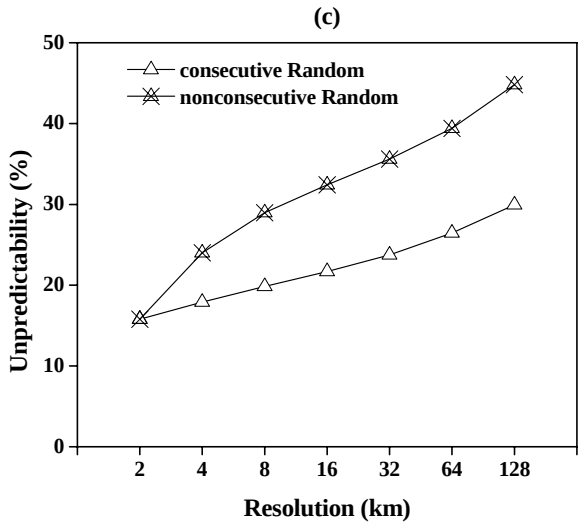

Figure 9. Assessment of unpredictability to illustrate algorithm performance. (a) Ranked aggregation − unpredictability is caused by the presence of random selections between classes due to equal γ-values. (b) Majority aggregation − unpredictability is caused by the presence of $\{2,2,0,0\}_a$, $\{2,2,0,0\}_d$, or $\{1,1,1,1\}$ block types. (c) Random aggregation − unpredictability is present in case of the heterogeneous block types.

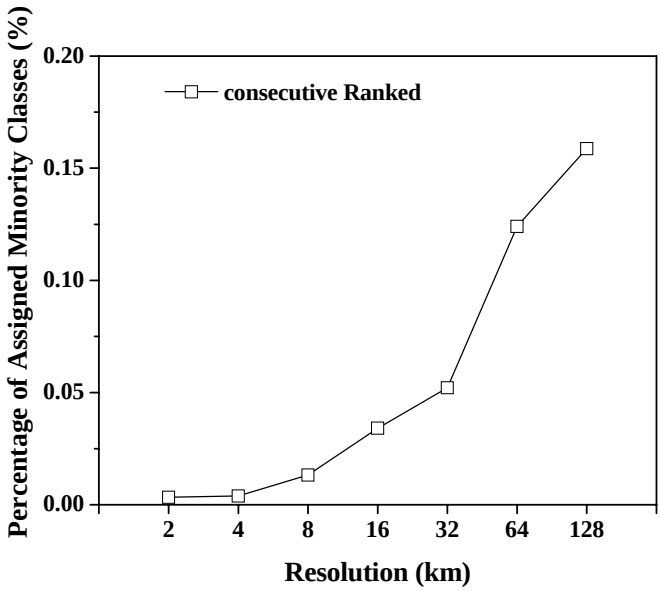

Figure 10. Block assignment to a minority class as a parameter of algorithm performance. Minority assignment is observed for block types $\{1,1,2,0\}_a$, $\{1,1,2,0\}_d$, and $\{1,3,0,0\}$.

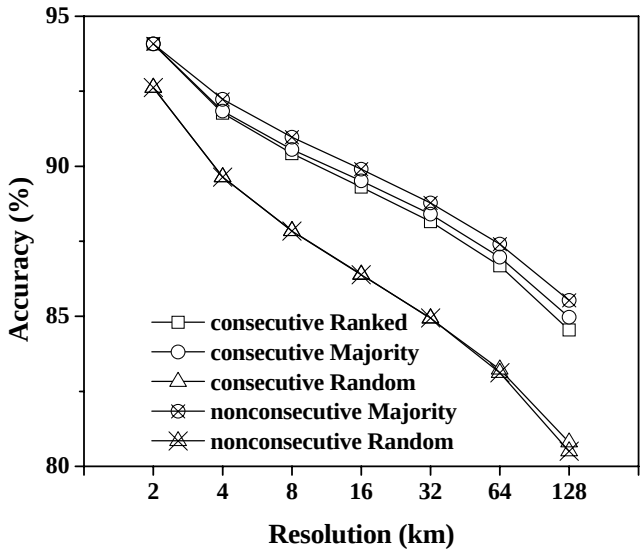

Figure 11. Accuracy of images aggregated using various aggregation algorithms.